MAGNETO-THERMOPOWER IN $MoSe_2$ MONOLAYER

Tran Ngoc Bich[1,2], Le Dinh[1], and Huynh Vinh Phuc[3*]

[1]Physics Department, University of Education, Hue University

[2]Faculty of Basic Sciences, Quang Binh University

[3]Faculty of Natural Sciences Teacher Education, Dong Thap University

[*]Corresponding author: Huynh Vinh Phuc, Email: hvphuc@dthu.edu.vn

Article history

Received: 27/9/2021; Received in revised form: 20/12/2021; Accepted: 07/3/2022

Abstract

We study the influence of the external magnetic field, temperature, and electron concentration on the magneto-thermopower due to the phonon-drag effect, S_{xx}^{g}, in the $MoSe_2$ monolayer. The analytical expression for S_{xx}^{g} is found from Π-method. Our numerical results show that the density of state and S_{xx}^{g} show an oscillation as a function of a magnetic field with its amplitude increases in the large magnetic field region. The S_{xx}^{g} increases with temperatures but decreases with electron concentrations. The numerical calculations for S_{xx}^{g} are compared with those in the graphene monolayer.

Keywords: *Electron-acoustic phonon interaction, magneto-thermopower, $MoSe_2$ monolayer.*

DOI: https://doi.org/10.52714/dthu.12.5.2023.1069

Cite: Tran, N. B., Le, D., & Huynh, V. P. (2023).. Magneto-thermopower in $MoSe_2$ monolayer. *Dong Thap University Journal of Science. 12*(5), 35-41. https://doi.org/10.52714/dthu.12.5.2023.1069.

CÔNG SUẤT NHIỆT-TỪ TRONG $MoSe_2$ ĐƠN LỚP

Trần Ngọc Bích[1,2], Lê Đình[1] và Huỳnh Vĩnh Phúc[3*]

[1]Khoa Vật lý, Trường Đại học Sư phạm, Đại học Huế

[2]Khoa Khoa học Cơ bản, Trường Đại Quảng Bình

[3]Khoa Sư phạm Khoa học tự nhiên, Trường Đại học Đồng Tháp

[*]Tác giả liên hệ: Huỳnh Vĩnh Phúc, Email: hvphuc@dthu.edu.vn

Lịch sử bài báo

Ngày nhận: 27/9/2021; Ngày nhận chỉnh sửa: 20/12/2021; Duyệt đăng: 07/3/2022

Tóm tắt

Chúng tôi khảo sát ảnh hưởng của từ trường ngoài, nhiệt độ, nồng độ electron lên công suất nhiệt-từ do hiệu ứng phonon-drag, S_{xx}^{g}, trong $MoSe_2$ đơn lớp. Kết quả giải tích của S_{xx}^{g} được thu nhận từ phương pháp Π. Kết quả tính số của chúng tôi cho thấy rằng mật độ trạng thái và S_{xx}^{g} dao động theo từ trường với biên độ tăng lên trong khoảng từ trường lớn. S_{xx}^{g} tăng theo nhiệt độ nhưng giảm theo nồng độ electron. Kết quả tính số này được so sánh với kết quả thu được trong graphene.

Từ khóa: *Tương tác electron-phonon âm, công suất nhiệt-từ, $MoSe_2$ đơn lớp.*

1. Introduction

In recent years, interest in studying graphene, a two-dimensional (2D) layer of graphite, has developed speedily due to its extraordinary electronic and optical properties as well as its potential applications in optical-electronic devices (Novoselov et al., 2005). The layered materials provide a flexible platform to explore fundamental physics and potential applications by combining different two-dimensional (2D) crystals (Geim and Grigorieva, 2013; Gang Wang et al., 2018). Among these kinds of materials, transition metal dichalcogenides are particularly suitable for basic and applied optics, as they are semiconductors with direct band dividers when thinned into monolayers (Mak et al., 2010).

In a recent work, Back et al., (2017) reported a strong paramagnetic response of a two-dimensional electron system (2DES) in a charge-tunable monolayer $MoSe_2$ sandwiched between two hexagonal boron-nitride (h-BN) layers. Their results showed that a magnetic field of 7 T leads to a near-complete valley polarization of electrons in a $MoSe_2$ monolayer with a density $n_e = 1.6\times10^{12}$ cm^{-2}. Chow et al. (2017) investigated the role of exciton–phonon interaction in exciton dynamics using the model system of monolayer $MoSe_2$. They showed that the neutral exciton photoluminescence intensity oscillates as a function of the excitation energy with a period matching that of the longitudinal negative phonon at the M-point.

It is well-known that two main parts contributing to the thermopower are electron diffusion and phonon-drag. The diffusion thermopower, S^d, is originated from the electron drift motion caused by either a temperature gradient or an electric field. Meanwhile, the phonon-drag thermopower, S^g, is generated as a result of the interaction between electrons and phonons (Kubakaddi et al., 1989; Biswas & Ghosh 2013). There exist in the literature two ways to obtain the phonon-drag thermopower S_{xx}^g known as "Q-method" by Cantrell and Butcher (1987a; 1987b), and "π-method" by Herring (1954). By establishing the fundamental relationship between their formulas, Tsaousidou et al. (2001) verified that these two methods are equivalent. Nonetheless, since π-method allows to establish a straightforward relation between the phonon-drag thermopower, S_{xx}^g, and the acoustic phonon-limited mobility, μ_{ac}, Herring's formula can be used to directly estimate the μ_{ac}, from the S_{xx}^g data (Tieke et al., 1998). For this reason, the π-method has been used to study the phonon-drag thermopower in 2DEG (Biswas and Ghosh 2013) and in graphene (Kubakaddi et al., 2017). In this work, we find the analytical expression of the thermopower due to phonon-drag effect in $MoSe_2$ monolayer in the presence of a magnetic field. The effects of temperature, the magnetic field, and the electron concentration on the thermopower are discussed in detail.

2. Expression for magneto-thermopower in $MoSe_2$ monolayer

Let consider a $MoSe_2$ sheet oriented in the (*xy*)-plane. In the presence of a perpendicular magnetic field $\vec{B}(x,y) = (0,0,B)$, Hamiltonian of the system is given as follows (Hien et al., 2020; Bich et al., 2021)

$$H = v_F\left(\tau\sigma_x\pi_x + \sigma_y\pi_y\right) + \Delta_{\tau,s}\sigma_z + \kappa_{\tau,s}, \qquad (1)$$

where $\tau = \pm 1$ is the valley index for *K* and *K*' valley, respectively, σ_x, σ_y, and σ_z are Pauli matrices, $\vec{\pi} = (\vec{p} + e\vec{A})$ is canonical momentum with $\vec{A} = (0, Bx, 0)$ is the vector potential of the magnetic field, $\Delta_{\tau,s} = \Delta/2 - (\lambda_v - \lambda_c)\tau s/4$, and $\kappa_{\tau,s} = (\lambda_v + \lambda_c)\tau s/4$, with $s = \pm 1$ being the spin index, Δ relating to energy gap, λ_c and λ_v being the spin splitting energy for the conduction and valence bands, respectively. The corresponding energy spectrum is

$$E_\alpha = E_{n,s}^{p,\tau} = \kappa_{\tau,s} + pE_{n,s}^{\tau}, \qquad (2)$$

where $n = 0,1,2,...$ is the Landau level (LL) index, $p = \pm 1$ is for the conduction and valence bands, respectively, and $E_{n,s}^{\tau} = \left[n(\hbar\omega_c)^2 + (\Delta_{\tau,s})^2\right]^{1/2}$ with $\omega_c = v_F\sqrt{2}/\alpha_c$ being the cyclotron frequency, $\alpha_c = (\hbar/eB)^{1/2}$ being the magnetic length. The corresponding wave functions for the *K* valley are

$$\psi_{n,s}^{\tau,p}(x,y) = \frac{e^{ik_y y}}{\sqrt{L_y}}\begin{pmatrix} A_{n,s}^{\tau,p}\phi_{n-1}(x-x_0) \\ iB_{n,s}^{\tau,p}\phi_n(x-x_0)\end{pmatrix}. \qquad (3)$$

Here, $\phi_n(x-x_0)$ is the normalization harmonic function centered at $x_0=\alpha_c^2 k_y$, and

$$A_{n,s}^{\tau,p}=\sqrt{\frac{pE_{n,s}^{\tau}+\Delta_{n,s}}{2pE_{n,s}^{\tau}}},B_{n,s}^{\tau,p}=\sqrt{\frac{pE_{n,s}^{\tau}-\Delta_{n,s}}{2pE_{n,s}^{\tau}}}. \quad (4)$$

The corresponding wave functions for *K'* valley are also derived from Eq. (3) but with replacing ϕ_{n-1} by ϕ_n. The density of state (DoS) is given as (Biswas & Ghosh, 2013)

$$D(\varepsilon)=\frac{1}{2\pi^2\alpha_c^2}\sum_{\eta}\frac{\gamma_L}{(\varepsilon-E_\eta)^2+\gamma_L^2}, \quad (5)$$

where $\gamma_L=\gamma\sqrt{B}$ is the Lorentz broadening with γ being calculated in the unit of meV $T^{-1/2}$.

When the electron-phonon interaction is taken into account, the magneto-thermopower due to phonon-drag effect, S_{xx}^{g}, is given as follows (Kubakaddi et al., 2017)

$$S_{xx}^{g}=-\frac{\rho_{yx}M_{yx}}{T}, \quad (6)$$

where ρ_{yx} is the Hall resistivity, T is the absolute temperature and

$$M_{yx}=\frac{e\alpha_c^2}{Sk_BT}\sum_{\vec{q}}v_s\tau_q\hbar\omega_q\left(\frac{q_y^2}{q}\right)K_{\alpha\alpha'}(q), \quad (7)$$

where S is the area of the system, $\omega_q=v_s q$ is the phonon frequency with v_s being the sound velocity, $\vec{q}=(q_x,q_y)$ being the phonon wave vector, τ_q is the phonon relaxation time, and

$$K_{\alpha\alpha'}(q)=\frac{2\pi}{\hbar}\sum_{\alpha,\alpha'}f(E_\alpha,E_{\alpha'})|C(q)|^2\left|J_{\eta',\eta}(u)\right|^2 \times N_q\delta(E_{\alpha'}-E_\alpha-\hbar\omega_q)\delta_{k_y',k_y+q_y}. \quad (8)$$

Here, $f(E_\alpha,E_{\alpha'})=f(E_\alpha)\left[1-f(E_{\alpha'})\right]$, the matrix element $C(q)$ describes the electron-phonon interaction length, $J_{\eta',\eta}(u)$ is the form factor with $u=\alpha_c^2q^2/2$, and $N_q=\left(e^{\hbar\omega_q/k_BT}-1\right)^{-1}$ is the phonon distribution function. We consider the S_{xx}^{g} in the low-temperature region where the interaction between electron and acoustic phonon is dominant. In this case, the matrix element for the electron-acoustic phonon interaction is given as follows

$$|C(q)|^2=\frac{\hbar D_{ac}^2 q}{2S\rho_m v_s}, \quad (9)$$

where ρ_m is area mass density and D_{ac} is coupling constant. Inserting the above expressions into Eq. (7), we get

$$M_{yx}=\frac{e\tau_q\hbar D_{ac}^2 v_s}{8\pi\rho k_BT}\sum_{\eta}\int_0^{\infty}dqq^4N_q\left|J_{\eta\eta}(u)\right|^2G_{\eta\eta}(q). \quad (10)$$

In Eq. (10) we have denoted

$$\left|J_{\eta\eta}(u)\right|^2=e^{-u}\left[(A_{n,s}^{\tau,p})^2L_{n-1}(u)+(B_{n,s}^{\tau,p})^2L_n(u)\right], \quad (11)$$

$$G_{\eta\eta}(q)=\int d\varepsilon\delta(\varepsilon-E_\eta)\delta(\varepsilon-E_{\eta'}+\hbar\omega_q) \times f(\varepsilon)\left[1-f(\varepsilon+\hbar\omega_q)\right], \quad (12)$$

where $L_n(u)$ are the Laguerre polynomials. Inserting Eq. (10) into Eq. (6) we obtain

$$S_{xx}^{g}=-\frac{\Lambda_p\hbar D_{ac}^2B}{8\pi n_e\rho k_BT^2}\sum_{\eta}\int_0^{\infty}dqq^4N_q\left|J_{\eta\eta}(u)\right|^2G_{\eta\eta}(q), \quad (13)$$

where $\tau_q=\Lambda_p/v_s$ with Λ_p being the phonon-free path. We can see that the result for S_{xx}^{g} as shown in Eq. (13) has the same form as that in graphene (Kubakaddi et al., 2017).

3. Numerical results and discussions

In this section, we present the numerical calculations on the S_{xx}^{g} in the $MoSe_2$ monolayer. The parameters used for the numerical calculations are given as follows (Mak et al., 2010; Hien et al., 2020; Bich et al.; 2021): $\hbar v_F=3.11$ eVA^0, $\Delta=0.74$ eV, $\lambda_v=0.184$ eV, $\lambda_c=-0.021$ eV, $D_{ac}=3.4$ eV, $\rho=2.01\times10^{-6}$ kg m^{-2}, $v_s=4.1\times10^3$ m/s, and $\Lambda_p=10^{-5}$ m. For convenience, we denote $n_0=10^{12}$ cm^{-2}.

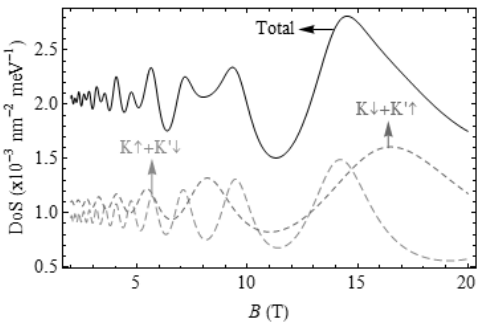

Figure 1. The density of states at Fermi level, $D(\varepsilon_F)$, as a function of magnetic field at $n_e=n_0$ and $\gamma=0.2$

In Fig. 1, we show the dependence of the density of state on the magnetic field for different electron states. Here, $K\uparrow+K'\downarrow$ and $K\downarrow+K'\uparrow$ are for the states with $\tau s=1$ and $\tau s=-1$, respectively. It is seen that the DoS displays an oscillatory behavior with the magnetic field in which their amplitudes increase with the increase of the magnetic field. This result is well-aligned with that reported in graphene (Kubakaddi *et al.*, 2017). Besides, given its large spin-orbit interaction coupling, the DoS in $MoSe_2$ are significantly separated. Since the energy for the $\tau s=1$ state is smaller than that for $\tau s=-1$, the number of oscillations due to that state $\tau s=1$ is bigger than that due to the state $\tau s=-1$.

In Fig. 2, we show the thermopower for different states as a function of the magnetic field. We can see that S_{xx}^{g} for both states with $\tau s=\pm 1$ display oscillatory behavior with a magnetic field. This result is in good agreement with that reported in conventional systems (Biswas & Ghosh, 2013) and in graphene monolayer (Kubakaddi et al., 2017). It is clear that, due to the strong SOC in $MoSe_2$, the contribution to S_{xx}^{g} from different states with $\tau s=\pm 1$ is completely separated, where the contribution from states with $\tau s=-1$ is bigger but less number of peaks in comparison to those from states with $\tau s=1$. This oscillatory behavior of the thermopower has a closed relation with that of DoS as shown in Fig. 1. Note that this separation behavior does not observe in graphene (Kubakaddi et al., 2017) because of the fact that in graphene, the SOC is very weak.

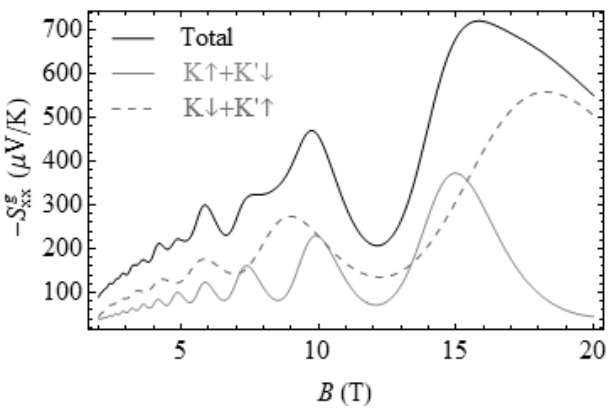

Figure 2. Magneto-thermopower, S_{xx}^{g}, as a function of the magnetic field at $n_e=n_0$ and $\gamma=0.2$

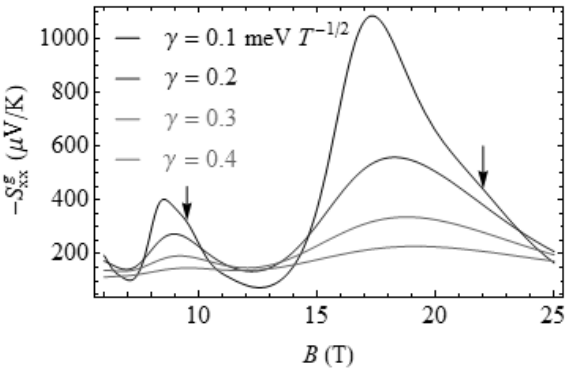

Figure 3. Magneto-thermopower, S_{xx}^{g}, as a function of the magnetic field for different Landau broadening parameters at $n_e=n_0$, $\tau s=-1$, and T=2 K

In Fig. 3, we show the influence of the Lorentz broadening parameter, γ, on the profile of the magneto-thermopower. We can see that when the γ increases the width (height) of the oscillation peak increases (decreases). This can be explained as follows: when the γ increases, the peaks become broader leading to the reduce of their amplidue. For small values of γ (indicating by vertical arrows), the minor peaks are observed significantly. These minor peaks will disappear when γ increases because in this case, the minor peaks contribute to the sum to generate the wider peak, similar to that of the resistivity in graphene (Greenaway et al., 2019).

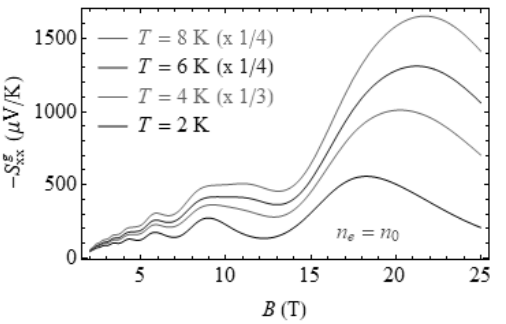

Figure 4. Magneto-thermopower, S_{xx}^{g}, as a function of the magnetic field for different temperatures at $\gamma=0.2$, $\tau s=-1$, and $n_e=n_0$

Figure 4 shows the thermopower as a function of magnetic field for different temperature. The results are calculated at $\gamma=0.2$, $\tau s=-1$, and $n_e=n_0$. For convenience, the results for T = 4, 6, and 8 K are multiplied by a corresponding factor. We can see that when the temperature increases both the width and amplitude of the oscillatory

peaks increase, which supports the results obtained in graphene (Kubakaddi *et al.*, 2017).

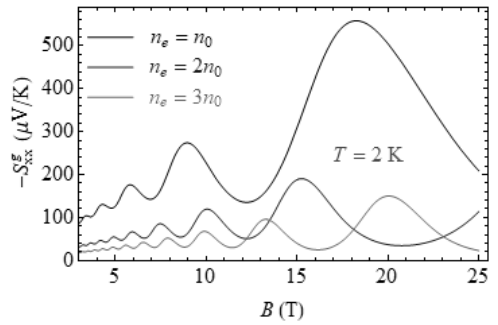

Figure 5. Magneto-thermopower, S_{xx}^g, as a function of the magnetic field for different electron concentrations at $\gamma = 0.2$, $\tau s = -1$, and T = 2 K

In Fig. 5, we show the dependence of the magneto-thermopower on the magnetic field for different electron concentrations at $\gamma = 0.2$, $\tau s = -1$, and T = 2 K. It can be seen that when the electron concentration increases, the amplitude of S_{xx}^g decreases. This can be explained directly from Eq. (13) that S_{xx}^g is proportional to the n_e^{-1}. Besides, the numbers of oscillation peaks also reduce with the increase of electron concentration. This can be explained by the fact that the oscillation frequency of the density of states is directly proportional to the electron density. Therefore, when the electron concentration increases, the oscillation peak position (of the same order) appear at the higher magnetic field range. Consequently, at a given range of the magnetic field, the numbers of oscillation peaks increase with the increase of the electron concentration. This has also been observed in 2D conventional systems (Biswas & Ghosh 2013) and graphene monolayer (Kubakaddi et al., 2017).

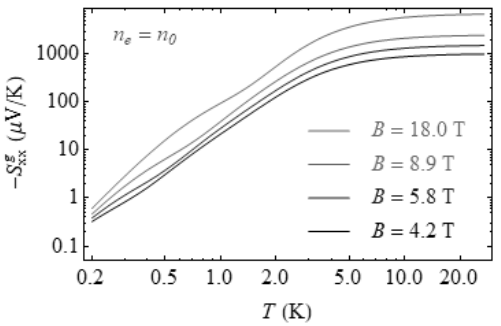

Figure 6. Magneto-thermopower, S_{xx}^g, as a function of the temperature for different magnetic fields at $\gamma = 0.2$, $\tau s = -1$, and $n_e = n_0$

In Fig. 6, we show the S_{xx}^g, due to the contribution from the states of $\tau s = -1$, as a function of the temperature for different magnetic fields. The values of the magnetic field of B = 4.2, 5.8, 8.9, and 18.0 T correspond to the peaks as shown in Fig. 4. We can see that S_{xx}^g increases with the increase of temperature: in the low-temperature region, the S_{xx}^g increases rapidly, then S_{xx}^g increases slowly and reaches its saturation value at about T = 10 K. This confirms the results reported in graphene (Kubakaddi et al., 2017). Besides, the amplitude of S_{xx}^g is higher for the higher magnetic fields.

The S_{xx}^g as a function of temperature for different n_e is shown in Fig. 7 at B = 5.8 T. We can see that when the electron concentration increases the thermopower decreases, being in agreement with that shown in Fig. 5.

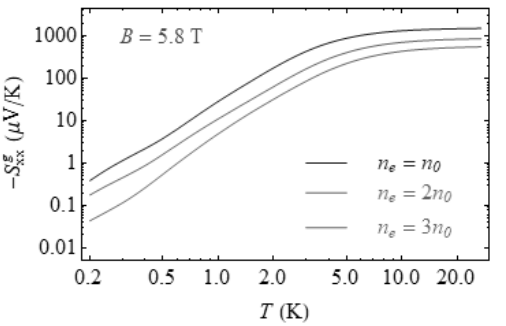

Figure 7. Magneto-thermopower, S_{xx}^g, as a function of the temperature for different electron concentrations at $\gamma = 0.2$, $\tau s = -1$, and B = 5.8 T

4. Conclusion

We have studied the influence of the magnetic field, temperature, and electron concentration on the magneto-thermopower in the $MoSe_2$ monolayer. We found an oscillatory behavior of S_{xx}^g with the magnetic field. The magneto-thermopower increases with the increase of temperature but decreases with electron concentration. In contrast to what happens in graphene, since the spin-orbit coupling in $MoSe_2$ is significantly strong, the oscillatory peaks due to different spin orientations are different. At the moment, we do not find any experimental data supporting our predations. However, our results about the S_{xx}^g, with the values up to few mV/K, are in good agreement with experimental data observed in MoS_2 (Buscema et al., 2013), another member of TMDC family materials.

References

Back, P., Sidler, M., Cotlet, O., Srivastava, A., Takemura, N., Kroner, M., & Imamoğlu, A. (2017). Giant paramagnetism-induced valley polarization of electrons in charge-tunable monolayer MoSe2. *Physical Review Letters*, 118(23), 237404. DOI: 10.1103/PhysRevLett.118.237404.

Bich, T. N., Kubakaddi, S. S., Dinh, L., Hieu, N. N., & Phuc, H. V. (2021). Oscillations of the electron energy loss rate in two-dimensional transition-metal dichalcogenides in the presence of a quantizing magnetic field. *Physical Review B*, 103(23), 235417. DOI: 10.1103/PhysRevB.103.235417.

Biswas, T., & Ghosh, T. K. (2013). Phonon-drag magnetothermopower in Rashba spin-split two-dimensional electron systems. *Journal of Physics: Condensed Matter*, *25*(41), 415301. DOI: 10.1088/0953-8984/25/41/415301.

Buscema, M., Barkelid, M., Zwiller, V., van der Zant, H. S., Steele, G. A., & Castellanos-Gomez, A. (2013). Large and tunable photothermoelectric effect in single-layer MoS2. *Nano Letters*, *13*(2), 358-363. DOI: 10.1021/nl303321g.

Cantrell, D. G., & Butcher, P. N. (1987a). A calculation of the phonon-drag contribution to the thermopower of quasi-2D electrons coupled to 3D phonons. I. General theory. Journal of Physics C: *Solid State Physics*, *20*(13), 1985. DOI: 10.1088/0022-3719/20/13/014.

Cantrell, D. G., & Butcher, P. N. (1987b). A calculation of the phonon-drag contribution to the thermopower of quasi-2D electrons coupled to 3D phonons. II. Applications. *Journal of Physics C: Solid State Physics*, *20*(13), 1993. DOI: 10.1088/0022-3719/20/13/015.

Chow, C. M., Yu, H., Jones, A. M., Schaibley, J. R., Koehler, M., Mandrus, D. G., Merlin, R., Yao, W., & Xu, X. (2017). Phonon-assisted oscillatory exciton dynamics in monolayer MoSe2. *NPJ 2D Materials and Applications*, *1*(1), 1-6. DOI: 10.1038/s41699-017-0035-1.

Gang, W., Chernikov, A., Glazov, M. M., Heinz, T. F., Marie, X., Amand, T., & Urbaszek, B. (2018). Colloquium: Excitons in atomically thin transition metal dichalcogenides. *Reviews of Modern Physics*, *90*, 021001. DOI: 10.1103/RevModPhys.90.021001.

(2018). Colloquium: Excitons in atomically thin transition metal dichalcogenides. *Reviews of Modern Physics*, *90*, 021001. DOI: 10.1103/RevModPhys.90.021001.

Geim, A. K., & Grigorieva, I. V. (2013). Van der Waals heterostructures. *Nature*, *499*, 6. DOI: 10.1038/nature12385.

Greenaway, M. T., Kumar, R. K., Kumaravadivel, P., Geim, A. K., & Eaves, L. (2019). Magnetophonon spectroscopy of Dirac fermion scattering by transverse and longitudinal acoustic phonons in graphene. *Physical Review B*, *100*(15), 155120. DOI: 10.1103/PhysRevB.100.155120.

Herring, C. (1954). Theory of the thermoelectric power of semiconductors. *Physical Review*, *96*(5), 1163. DOI: 10.1103/PhysRev.96.1163.

Hien, N. D., Nguyen, C. V., Hieu, N. N., Kubakaddi, S. S., Duque, C. A, Mora-Ramos, M. E., Dinh, L., Bich, T. N., & Phuc, H. V. (2020). Magneto-optical transport properties of monolayer transition metal dichalcogenides. *Physical Review B*, *101*(4), 045424. DOI: 10.1103/PhysRevB.101.045424.

Kubakaddi, S., Biswas, T., & Ghosh, T. K. (2017). Phonon-drag magnetoquantum oscillations in graphene. *Journal of Physics: Condensed Matter*, *29*(30), 305301. DOI: 10.48550/arXiv.1702.01087.

Kubakaddi, S. S., Butcher, P. N., & Mulimani, B. G. (1989). Phonon-drag thermopower of a two-dimensional electron gas in a quantizing magnetic field. *Physical Review B*, *40*(2), 1377. DOI: 10.1103/PhysRevB.40.1377.

Mak, K. F., Lee, C., Hone, J., Shan, J., & Heinz, T. F. (2010). Atomically thin MoS2: A new direct-gap semiconductor. *Physical Review Letters*, *105*(13), 136805. DOI: 10.1103/PhysRevLett.105.136805.

Novoselov, K. S., Geim, A. K., Morozov, S. V., Jiang, D., Katsnelson, M. I., Grigorieva, I. V.,Dubonos, S., & Firsov, A. A. (2005). Two-dimensional gas of massless Dirac fermions in graphene. *Nature*, *438*(7065), 197-200. DOI: 10.1038/nature04233.

Tieke, B., Fletcher, R., Zeitler, U., Henini, M., & Maan, J. C. (1998). Thermopower measurements of the coupling of phonons to electrons and composite fermions. *Physical Review B*, *58*(4), 2017. DOI: 10.1103/PhysRevB.58.2017.

Tsaousidou, M., Butcher, P. N., & Triberis, G. P. (2001). Fundamental relationship between the Herring and Cantrell-Butcher formulas for the phonon-drag thermopower of two-dimensional electron and hole gases. *Physical Review B*, *64*(16), 165304. DOI: 10.1103/PhysRevB.64.165304.